Supporting Information

Size dependent efficiency of photophoretic swimmers

Andreas P. Bregulla, Frank Cichos

1 Janus particle images

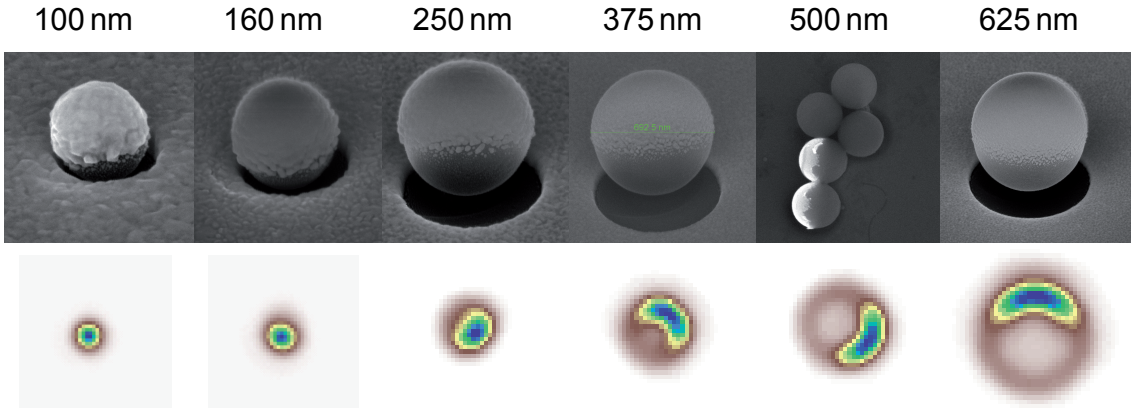

Figure 1: TEM image (top) of gold evaporated Janus particles in addition to its typical darkfield images (bottom) for each particle size.

2 Sample preparation

Samples consist of two glass cover slides, which were rinsed with acetone, ethanol and distilled water and treated with an oxygen plasma. They have been further coated with Pluronic F-127 (Sigma Aldrich) in a 5% aqueous solution for a few hours. The Pluronic is adsorbed to the glass surface and prevents sticking of the Janus particles to the glass surface due to electrostatic interactions. Residual Pluronic has been removed by rinsing the coated slides with distilled water. A dilute Janus particle solution was then deposited between the two slides and sealed with polydimethylsiloxane (PDMS) to prevent evaporation of the aqueous solution. The typical thickness of the liquid layer between the glass slides has been adjusted to be below $2\mu m$.

3 Experimental setup

The experimental setup (Fig. 2A) consist of two parts, the heating and the illumination part. For the heating part a common laser source at a wavelength of 532 nm was used. This beam was first enlarged by a beam expander and then focused by a lens into the back aperture of an oil immersion objective (Olympus 100x NA 0.5-1.3). This ensures a parallel beam after the objective with a beam-waist of $\approx 9\,\mu$m.
The illumination of the sample is realized by an oil immersion dark field condenser (Olympus NA 1.2-1.4). The scattered white light is collected by the objective and imaged on the CCD-camera (Andor iXon). For the spatial position of the sample a piezo-scanner was used (Physik Instrumente, PI).
The images obtained by the camera are processed and the information of the particles position and orientation are transferred to a programmable analog digital converter controlling the laser intensity and the positioning of the sample (AdWin, Jäger Messtechnik).

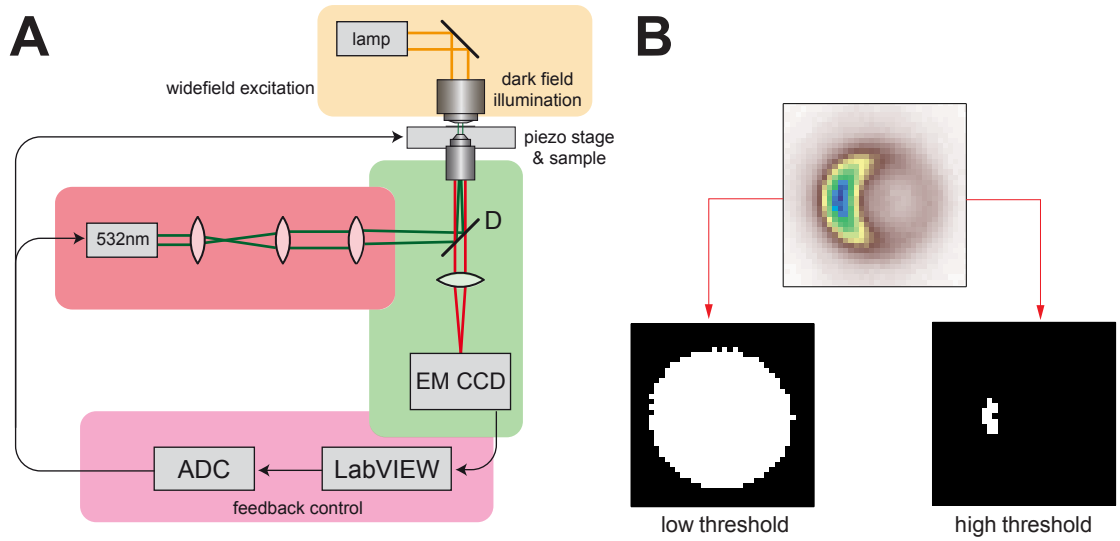

Figure 2: **(A)** Sketch of the optical microscope. **(B)** Principle of the determination of the particles position and orientation.

To obtain the phoretic velocity of the particles two different methods were used. Within the first method called photon nudging the position and orientation as displayed in Fig. 2B are obtained by two binary images. The first binary image is obtained at a threshold slightly above the background noise. Its center of mass determines the position of the particle. Together with the center of mass of the second binary image obtained at a threshold of about 90% of the maximum intensity the orientation can be calculated. In dependence of the position and orientation of the particle relative to the center of the camera image the laser heating is turned on when the particle's orientation is facing the target position and turned off if it is not.(for further details see ref. 1,2)
The second method is used for particles that are too small to obtain the orientation directly from the images. Here only the position was detected by the center of mass of the first binary image and accordingly to this position relative to the center of the image the piezo-stage was moved to keep the particle within the region of interest.

4 Mean squared displacement

Here the MSD for the 2D projection of a 3D rotational correlated directed motion is calculated similar to Schienbein *et. al.*[3] The following calculation is adapted to the system studied here.
The projected velocity vector reads:

$$\vec{V}_{th}(t) = \begin{pmatrix} v_x(t)\cos(\phi(t)) \\ v_y(t)\sin(\phi(t)) \end{pmatrix} \tag{1}$$

$\phi(t)$ is here the projected angle of the particles orientation in the xy plane.
So the position of the particle is given by:

$$x(t) = \int_0^t v_x(t')\, Cos(\phi(t'))\, dt' \tag{2}$$

and the MSD reads then[4]

$$\left\langle x(t)^2 \right\rangle = \left\langle \left[\int_0^t v_x(t')\, Cos(\phi(t'))\, dt' \right]^2 \right\rangle \tag{3}$$

$$= 2\left\langle \int_0^t v_x(t_1)\, Cos(\phi(t_1))\, dt_1 \int_0^{t_1} v_x(t_2)\, Cos(\phi(t_2))\, dt_2 \right\rangle \tag{4}$$

Because $v_x(t)$ and $\phi(t)$ are independent from each other equation 4 can be rewritten into:

$$\left\langle x(t)^2 \right\rangle = 2\int_0^t \int_0^{t_1} \langle v_x(t_1)\, v_x(t_2)\rangle \langle Cos(\phi(t_1))\, Cos(\phi(t_2))\rangle\, dt_2\, dt_1 \tag{5}$$

For convenience at this point a constant velocity is assumed so that $\langle v_x(t_1)\, v_x(t_2)\rangle = V_{th}^2$

$$\left\langle x(t)^2 \right\rangle = 2V_{th}^2 \int_0^t \int_0^{t_1} \langle Cos(\phi(t_1))\, Cos(\phi(t_2))\rangle\, dt_2\, dt_1 \tag{6}$$

To calculate $\langle Cos(\phi(t_1))\, Cos(\phi(t_2))\rangle$ we obtain first the equation of motion for the angle $\phi(t)$. The orientation is in this case only driven by random forces.

$$\dot{\phi}(t) = \Gamma(t) \tag{7}$$

Here, $\Gamma(t)$ is a stochastic torque and therefore the following assumptions for this torque has to be fulfilled.

$$\langle \Gamma(t)\rangle = 0 \tag{8}$$

$$\langle \Gamma(t)\,\Gamma(t')\rangle = q_\phi \delta(t - t') \tag{9}$$

Whereby q_ϕ quantifies the strength of the stochastic torque. Because Eq.7 cannot predict the migration of the angle $\phi(t)$ of a single particle as a function of time one has to solve the corresponding Fokker Planck equation[5].

$$\hat{L}_{fp} W(\phi, t) = \frac{\partial W(\phi, t)}{\partial t} \tag{10}$$

with

$$\hat{L}_{fp} = \frac{\partial}{\partial \phi}\left(\frac{q_\phi}{2} \frac{\partial}{\partial \phi} \right) \tag{11}$$

To solve Eq.10 the following separation ansatz is assumed.

$$W(\phi, t) = \Theta(\phi) \exp(-\lambda t) \tag{12}$$

so that

$$\hat{L}_{fp}\Theta\left(\phi\right) = -\lambda\Theta\left(\phi\right) \tag{13}$$

Because the problem is 2π periodic $\Theta\left(\phi\right)$ can be expressed by a Fourier series.

$$\Theta\left(\phi\right) = \sum_{n=-\infty}^{\infty} c_n \exp\left(-i\, n\, \phi\right) \tag{14}$$

with $c_n = c^*_{-n}$ and $c_n = a_n + i\, b_n$.
By combining Eq.14 and Eq.13 one gets:

$$\left(\tilde{\lambda} - n^2\right) c_n = 0 \tag{15}$$

with $\tilde{\lambda} = 2\lambda/q_\phi$ and so the eigenvalues are:

$$\tilde{\lambda}_\mu = \mu^2 \tag{16}$$

with the eigenfunctions

$$\Theta_\mu = 2a^\mu_\mu \cos\left(\mu\phi\right) + 2b^\mu_\mu \sin\left(\mu\phi\right) \tag{17}$$

Θ_μ can be split into a symmetric and an asymmetric part $\Theta_\mu = \Theta^s_\mu + \Theta^a_\mu$ with

$$\Theta^s_\mu = 2a^\mu_\mu \cos\left(\mu\phi\right) \tag{18}$$

being the symmetric part and

$$\Theta^a_\mu = 2b^\mu_\mu \sin\left(\mu\phi\right) \tag{19}$$

the asymmetric part.
Because the Fokker Planck operator is hermitian all eigenfunctions for different eigenvalues are orthogonal:

$$\int_0^{2\phi} \left(\Theta^i_\mu\right)^2 \, d\phi = 1 \tag{20}$$

whereby the index i represents the symmetric or asymmetric case. With help of equation 20, equation 18 and 19 can be rewritten.

$$\Theta^s_\mu = \frac{1}{\sqrt{\pi}} \cos\left(\mu\phi\right) \tag{21}$$

$$\Theta^a_\mu = \frac{1}{\sqrt{\pi}} \sin\left(\mu\phi\right) \tag{22}$$

With those eigenfunctions now one can solve Eq.6 with the stationary solution $W_{st} = 1/2\pi$

$$\left\langle \cos\left(\phi\left(t_1\right)\right) \cos\left(\phi\left(t_2\right)\right)\right\rangle = \int_0^{2\pi} d\phi \cos\left(\phi\right) \int_0^{2\pi} d\phi' \cos\left(\phi'\right) W_{st} \sum_{\mu,i} \Theta^i_\mu\left(\phi\right) \Theta^i_\mu\left(\phi'\right) \exp\left(-\tilde{\lambda}_\mu\left(t_1 - t_2\right)\right) \tag{23}$$

$$= \frac{1}{2} Exp\left[-\frac{q_\phi\left(t1 - t2\right)}{2}\right] \tag{24}$$

with and $q_\phi = 2/\tau_R$ one gets the solution for the MSD Eq.6

$$\left\langle x\left(t\right)^2\right\rangle = V^2_{th}\tau^2_R\left(\frac{t}{\tau_R} + \exp\left(-\frac{t}{\tau_R}\right) - 1\right) \tag{25}$$

because for the given random walk x and y are independent variables the 2D MSD reads then:

$$\left\langle r\left(t\right)^2\right\rangle = 2V^2_{th}\tau^2_R\left(\frac{t}{\tau_R} + \exp\left(-\frac{t}{\tau_R}\right) - 1\right) \tag{26}$$

The velocity auto correlation is then half of the second derivative[6]:

$$\mathrm{VAC\,(t)} = \frac{\partial^2 \left\langle \mathrm{r\,(t)^2}\right\rangle}{\partial \mathrm{t^2}}/2 \tag{27}$$

$$\mathrm{VAC\,(t)} = \mathrm{V^2_{th}} \exp\left(-\frac{\mathrm{t}}{\tau_\mathrm{R}}\right) \tag{28}$$

5 Estimate of the phoretic velocity of 100 nm and 160 nm swimmers

5.1 160 nm

The velocity auto correlation of the experimentally obtained time traces of N particle position $\vec{x}_i$ was calculated using the following equation:

$$\mathrm{VAC}\,(\delta) = \frac{1}{N-\delta-1} \sum_{i=1}^{N-\delta-1} \vec{V}_i \cdot \vec{V}_{i+\delta} \tag{29}$$

with

$$\vec{V}_i = \left(\vec{x}_{i+1} - \vec{x}_i\right)/\Delta t \tag{30}$$

Δt beeing the inverse frame rate being equal to 5 ms.
Fig. 3A displays examples of VAC's as a function of the lagtime δ. Those curves were fitted with Eq. 28 and the obtained phoretic velocity is displayed in Fig. 3B. The individual points represent the calculated velocity for each individual particle. The black solid line is the average of all individual velocities at a certain heating power.

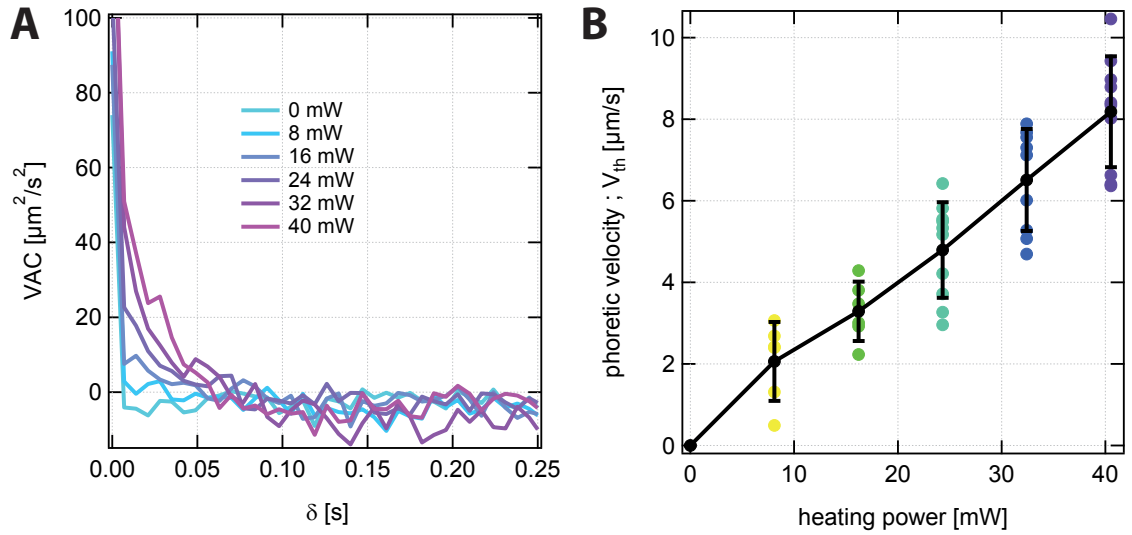

Figure 3: **(A)** Velocity correlation for a $R = 160$ nm Janus particle at different heating powers **(B)** Obtained thermophoretic velocity. Each point represents an individual particle.

5.2 100 nm

In the case of very small swimmers, the velocity auto correlation is not applicable since the rotational motion is significantly faster than the inverse frame rate. To estimate the phoretic velocity of these swimmers first the mean squared displacement was calculated using the following equation.

$$\mathrm{MSD}\,(\delta) = \frac{1}{N-\delta}\sum_{i=1}^{N-\delta}\left(\vec{x}_{i+\delta} - \vec{x}_i\right)^2 \tag{31}$$

The average MSD's are displayed in Fig. 4A as a function of the lagtime δ.
Corresponding to the linear slope of the long time limit of Eq. 26 the obtained MSD was fitted with $4D_{\mathrm{eff}}\delta$ (see Fig. 4B). The extracted effective diffusion coefficient D_{eff} consist out of the translational diffusion coefficient and the persistence length ($4D_{\mathrm{eff}} = 4\,D + 2V_{th}^2\tau_R$). The translational diffusion coefficient was obtained for zero heating power. Its value is reduced compared to the theoretical value D_0 basically due to the thin sample geometry. To calculate the phoretic velocity the knowledge of the rotational timescale τ_R is needed. For these particles the theoretical value for a $R = 125\,nm$ colloid is assumed (radius of polystyrene sphere + half of the cap thickness). The extracted phoretic velocity is display in Fig .4.

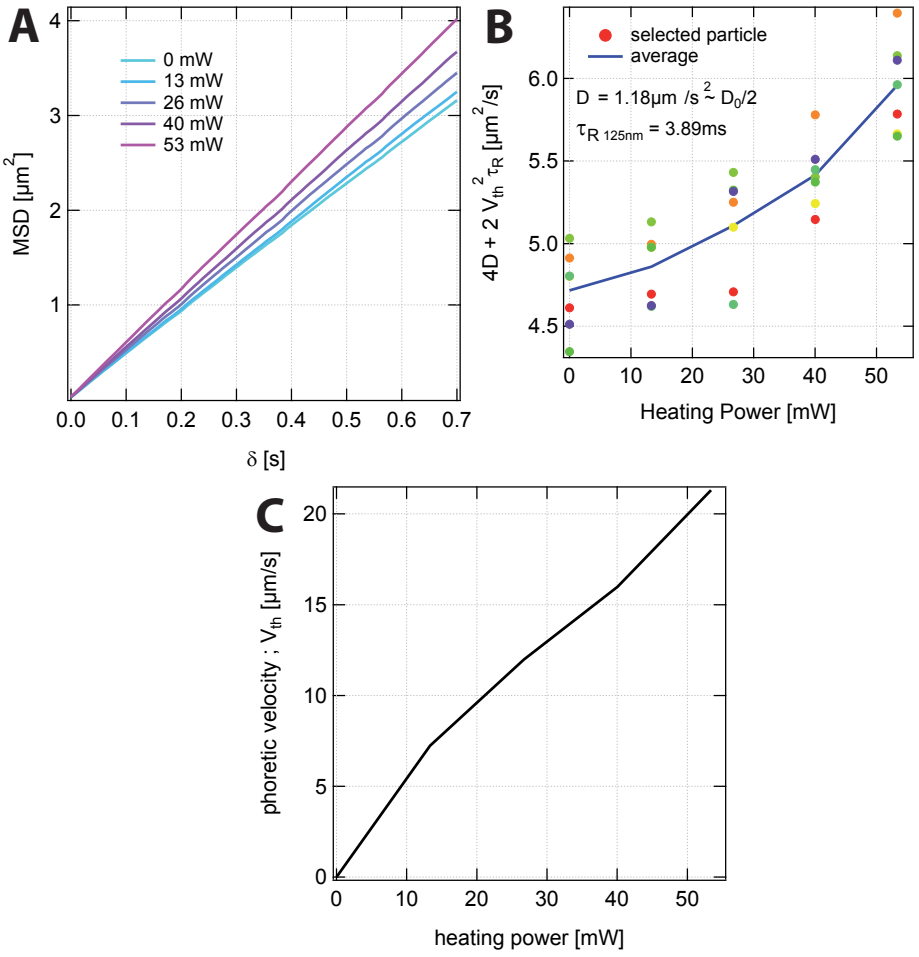

Figure 4: **(A)** Mean squared displacement for a $R = 100\,\mathrm{nm}$ Janus particle at different heating powers **(B)** Obtained effective diffusion coefficient D_{eff}. Each point represents an individual particle.**(C)** Average phoretic velocity V_{th} as a function of the heating power.

6 Simulation of the surface temperature gradient.

Numerical simulations of the temperature gradient at the Janus particle surface where carried out with help of Comsol 4.2.
The stationary heat conduction equation was solved

$$\kappa \nabla^2 T + Q_V = 0 \tag{32}$$

with Q_V being the heat source density. The gold cap was set to be the heat source of the Janus particle with an absorbed power density of

$$Q_V = \frac{P_{abs}}{V_{cap}} \tag{33}$$

$$V_{cap} = \frac{2}{3}\pi \left((R + \Delta r)^3 - R^3 \right) \tag{34}$$

$$P_{abs} = I\, \sigma_{abs} \tag{35}$$

$$Q_V = \frac{3}{2\pi} \frac{I\, \sigma_{abs}}{\left((R + \Delta r)^3 - R^3 \right)} \tag{36}$$

Q_V ...	absorbed power per Volume	P_{abs} ...	absorbed power
I ...	incident Intensity	σ_{abs} ...	absorption cross section
V_{cap} ...	volume of the cap	R ...	radius of polystyrene sphere
Δr ...	thickness of cap	κ ...	thermal conductivity [W/m K]

In the following a constant incident intensity $I_{inc} = \text{const}$ was assumed.
The thermal conductivities are $\kappa_{ps} = 0.08\,\mathrm{W/(m\,K)}$ for polystyrene, $\kappa_{water} = 0.6\,\mathrm{W/(m\,K)}$ for water and $\kappa_{Au} = 320\,\mathrm{W/(m\,K)}$ for gold.

7 Size dependent scattering and absorption cross section of gold colloids

The following absorption and scattering cross sections were obtained using open source software MiePlot [7]. The gold colloid was thereby embedded in water and illuminate with a plane wave. The refractive index of gold at a wavelength of 532 nm was set to $n_{Au} = 0.5445 + 2.23\mathrm{i}$ and to $n = 1.335$ for water.

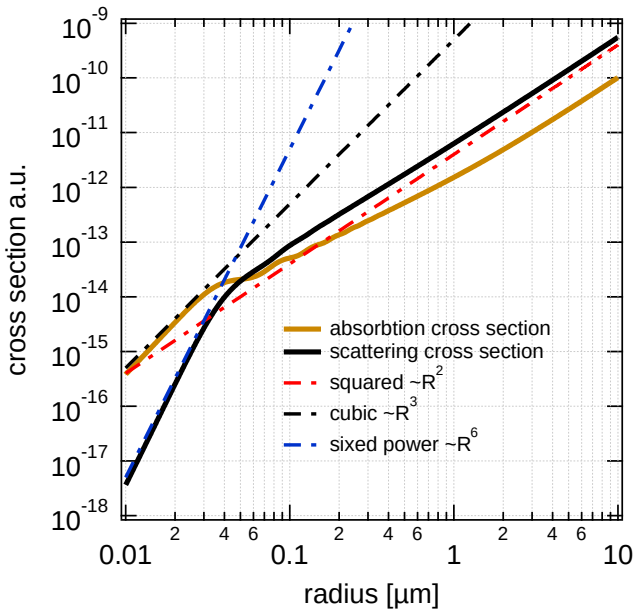

Figure 5: Scattering and absorption cross section of a gold colloid illuminated by a plane wave at a wavelength of 532 nm as a function of the particle radius.

For small particle sizes the scattering cross section scales with the volume squared and therefore with $\sigma_{sca} \propto R^6$ while the absorption cross section scales with the volume of the gold colloid, thus $\sigma_{abs} \propto R^3$. In the limit of large particles for cross section scale with the surface of the colloid ($\sigma_{abs} \propto R^2$; $\sigma_{sca} \propto R^2$) as visible in Fig. 5. The dependence of σ_{abs} for intermediate particle sizes is however more complex due to plasmonic resonances.

References

[1] B. Qian, D. Montiel, A. Bregulla, F. Cichos and H. Yang, *Chem. Sci.*, 2013, **4**, 1420–1429.

[2] A. P. Bregulla, H. Yang and F. Cichos, *ACS Nano*, 2014, **8**, 6542–6550.

[3] M. Schienbein and H. Gruler, *Bulletin of Mathematical Biology*, 1993, **55**, 585–608.

[4] A. W. and G. Hoffmann, *InLecture Notes in Biomathematics. Biological Motion*, 1990, 254–268.

[5] H. Risken, *The Fokker-Planck Equation.*, Heidelberg Springer Verlag., 1984.

[6] H. Qian, M. Sheetz and E. Elson, *Biophysical Journal*, 1991, **60**, 910 – 921.

[7] P. Laven, *Appl. Opt.*, 2003, **42**, 436–444.